

MORPHOLOGICAL SIGNATURES OF NONGAUSSIANTY IN CMB MAPS

S.F. SHANDARIN

*Department of Physics and Astronomy, University of Kansas,
1082 Malott Hall, 1251 Wescoe Hall Dr., Lawrence, KS 66045, U.S.A.*



The morphological tests of the Gaussianity of CMB maps are briefly described. The quadratic model being often referred to as physically motivated type of nonGaussianity has a simple morphology analytically described in terms of the Gaussian Minkowski functionals. The morphology of the QMASK map having a FWHM angular resolution of 0.68° is consistent with the hypothesis of Gaussianity.

1 Introduction

The issue of Gaussianity of CMB maps plays a crucial role in testing assumptions about the early Universe. The simplest inflation models strongly favor Gaussianity of the primordial inhomogeneities (however, $\Delta T/T$ can be nonGaussian ⁷), whereas other scenarios assuming cosmic strings or topological defects predict non-Gaussian perturbations. Gaussianity is also a key underlying assumption of all experimental power spectrum analyses to date, entering into the computation of error bars ^{1,18}, and therefore needs to be observationally tested. Another reason for studying Gaussianity of CMB maps is that it may reveal otherwise undetected foreground contamination and/or possible spurious effects. It needless to say that the models of the structure formation critically depend on the assumptions about the type of the initial fluctuations.

We discuss here a set of morphological statistics sensitive to the nonGaussian patterns. One of the advantages of the morphological studies consists in a natural and easy separation of the information contained in the probability density function (hereafter pdf) which is the simplest statistic sensitive to nonGaussianity. Another useful property of morphological statistics is its intrinsic spatial localization which is very useful for understanding the nature of the nonGaussian signal ⁴. Finally, computing the morphological statistic is numerically efficient ($\propto N_{pix} \ln N_{pix}$) ¹⁷ which is very important for the analysis of large maps like MAP and PLANK.

2 Morphology of a Map

From a mathematical point of view every field $F(x, y)$ can be fully described with the help of a sufficiently large set of contour lines $F(x, y) = F_i$. An example is the set of contours of the temperature contrast $\Delta T/T$ in CMB maps. For a given set of contours the set of values labeling the contours determines all one point statistics (skewness, kurtosis, or the pdf itself). The information stored in the patterns made by the contour lines can be conveniently called morphology which includes both the geometry and topology of the field.

A true Gaussian map must have both the Gaussian morphology and Gaussian pdf. However, an arbitrary set of contour lines can be labeled to give exactly the Gaussian pdf but preserving the original morphology. Similarly the true Gaussian field can be relabeled to result in an arbitrary pdf but preserving the Gaussian morphology. If the relabeling is made by a monotonic transformation $v = G(u)$ (where u and v are respectively the initial and final fields, and the function G is monotonic) then the resulting map $v(x, y)$ has exactly the same morphology as the initial map $u(x, y)$.

Many nonGaussian fields are derived from one or more Gaussian fields. One example is the so called quadratic model (see *e.g.* ^{7,8,19}) and another a χ_n^2 field with n degrees of freedom. We shall discuss the quadratic model in more detail in Sec. 4.

3 Measuring the Morphology of a Map

Morphology of two-dimensional random fields can be conveniently described in terms of geometric and topological properties of the regions bounded by the contours of constant level. There is a particularly useful set of quantities called Minkowski functionals which have very simple geometric and topological interpretations. For each isolated region bounded by a contour there are only three scalar Minkowski functionals: the area within the boundary, a_i , its perimeter or the contour length, c_i , and the Euler characteristic or genus, $g_i = 1 - n_{hi}$ where n_{hi} is the number of holes in the region.

Minkowski functionals are additive quantities and make perfect sense for a separate region as well as for an arbitrary set of regions. They can be easily calculated for any set of regions if they are known for each region. In particular, the global Minkowski functionals, *i.e.* the total area, A , contour length, C and genus, G of the excursion set: $A = \sum_i a_i$, $C = \sum_i c_i$, $G = \sum_i g_i$ are often used ^{6,10,11,12,17,20,21}.

The total area of the excursion set, A as a function of the level is obviously the cumulative probability function (CPF) of the field: $A(u) \equiv P(u) = \int_u^\infty p(u') du'$. The Euler characteristic or genus have been used in cosmology for a number of years ^{2,3,5}.

The first time the set of global Minkowski functionals was introduced into cosmology with the reference to their significance in differential and integral geometry by Mecke, Buchert and Wagner ⁹. In particular, they emphasized a powerful theorem by Hadweiger stating that under rather broad restrictions the set of scalar, vectorial and tensorial Minkowski functionals provides a complete description of the morphology. In addition, the Minkowski functionals of the largest (by area) region (A_p , C_p , and G_p) give accurate description of the percolation phase transition ²⁴. At percolation the regions merge into one region that spans throughout the whole space of the field. Percolation phase transition is sensitive to some types on non-Gaussianity ^{13,15,16}.

4 Quadratic Model

Consider *e.g.* the quadratic model

$$v = u + \alpha(u^2 - 1) \quad (1)$$

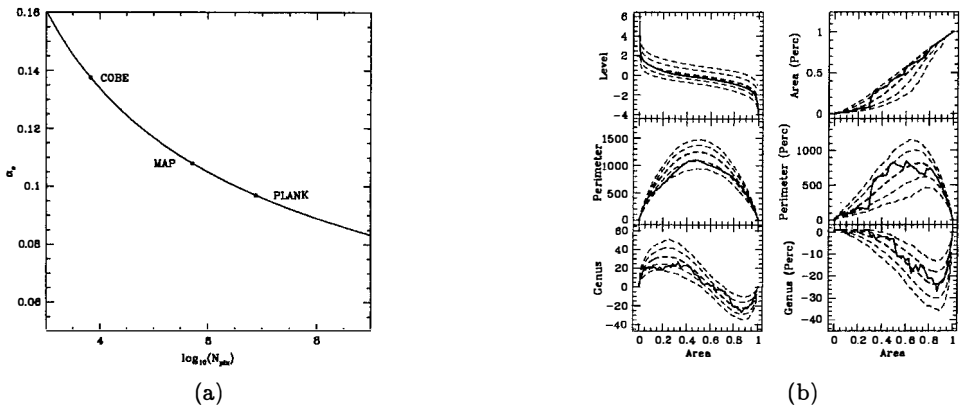


Figure 1: a) The critical amplitude α_c of the quadratic model as a function of the size of the map. Below the line $\alpha = \alpha_c$ the quadratic model has the Gaussian morphology and is fully described by the pdf. b) Minkowski functionals as functions of the fraction of the area in the excursion set, $A = A_{ES}/A_m$, where A_{ES} and $A_m = A_{ES}(-\infty)$ is the area of the excursion set and that of the whole map, respectively. The left hand side column from top to bottom: the level in σ s, contour length C and genus G of the excursion set. The right hand side column from top to bottom: the fraction area A_p , contour length C_p and G_p of the largest (*i.e.* percolating) cluster. The contour length is given in mesh units. The genus is “number of regions” – “number of holes”. The solid lines show the parameters of the QMASK map, heavy dashed lines show the median Gaussian values, thin dashed lines show 68% and 95% ranges.

where u is a Gaussian field with $\langle u \rangle = 0$, $\langle u^2 \rangle = 1$ and α is a constant. Parameter α is related to the f_{NL} parameter⁷ as $\alpha = \sigma_{\Phi_L} f_{NL}$ while $\Phi_L = \sigma_{\Phi_L} u$ and $\Delta T/T = -v\sigma_{\Phi_L}/3$. It is often referred to as one of the physically motivated types of nonGaussianity^{8,7,11,19}. Being formally nonmonotonic transformation of a Gaussian field the quadratic model effectively becomes monotonic if the amplitude α is small enough for a given size of the map. The critical value of the amplitude can be found from the following equation¹⁴

$$N_{pix} \approx \sqrt{\frac{\pi}{2}} \frac{1}{\alpha_c} \exp\left(\frac{1}{8\alpha_c^2}\right). \quad (2)$$

Fig. 1a shows the critical amplitude α_c for the COBE, MAP and PLANK experiments. The morphology in the quadratic model remains exactly Gaussian if $\alpha \leq \alpha_c$ and the existing non-Gaussianity can be detected by the pdf. The one-point statistics (skewness, and higher moments) can detect the amplitude two orders of magnitude smaller than the critical value on a $N_{pix} = 1024^2$ grid¹⁴. At a such amplitude the quadratic model has perfectly Gaussian morphology. At $\alpha > \alpha_c$ the morphology is not Gaussian anymore but remains fairly simple and can be analytically described in terms of the Minkowski functionals of the parent Gaussian field¹⁴.

5 QMASK

The QMASK map, described in²² (and references therein), combines all the information from the QMAP and Saskatoon experiments into a single map at 30-40 GHz covering about 648 square degrees around the North Celestial Pole. The map consists of sky temperatures in 6495 sky pixels, conveniently grouped into a 6495-dimensional vector \mathbf{x} , with a FWHM angular resolution of 0.68° . All the complications of the map making and deconvolution process are encoded in the corresponding 6495×6495 noise covariance matrix.

Along with the QMASK map we analyze a thousand reference maps with the same sky coverage, noise properties and power spectrum as the QMASK map.

Fig. 1b shows that the morphology of the QMASK map is compatible with the assumption of Gaussianity. A simple quantitative estimates confirm this observation¹⁷.

6 Summary

The properties of the Minkowski functionals such as a sensitivity to nonGaussian morphology, local character, and computational efficiency make them useful statistical tools complimentary to the n-point functions for testing the Gaussianity of CMB maps.

As many argued the quadratic model is physically motivated at the inflationary stage^{7,11,19}. The morphology of this model can be analytically described in terms of the Minkowski functionals of the Gaussian field for an arbitrary amplitude α ¹⁴. For a finite size map there is a critical amplitude α_c (eq. 2) separating the case of the exactly Gaussian morphology ($\alpha < \alpha_c$) from nonGaussian morphology.

The morphological tests has been applied to the QMASK map combining all the information from the QMAP and Saskatoon experiments into a single map at 30-40 GHz. It consists of sky temperatures in 6495 sky pixels and has a FWHM angular resolution of 0.68°. The morphology of the map is consistent with the hypothesis of Gaussianity of the initial fluctuations¹⁷.

References

1. J.R. Bond, A.H. Jaffe, in *Proc. XVI Rencontre de Moriond, Microwave Background Anisotropies*, ed. F. R. Bouchet (Paris: Editions Frontiers, 1998).
2. P. Coles, *MNRAS* **234**, 509 (1988)
3. A.G. Doroshkevich, *Astrophysics* **6**, 320 (1970)
4. P.G. Ferreira, J. Magueijo and J. Silk, *Phys. Rev. D* **56**, 7493 (1997)
5. J.R. Gott III, A.L. Melott and M. Dickinson, *ApJ* **306**, 341 (1986)
6. J.R. Gott III, C. Park, R. Juszkiewicz, W.E. Bies, D.P. Bennett, F.R. Bouchet, and A. Stebbins, *ApJ* **352**, 1 (1990)
7. E. Komatsu and D.N. Spergel, *Phys. Rev. D* **63**, 063002 (2001)
8. X. Luo, D.N. Schramm, *ApJ* **408**, 33 (1993)
9. K.R. Mecke, T. Buchert, H. Wagner, *ApJ* **288**, 697 (1994)
10. D. Novikov, H. Feldman, H., and S.F. Shandarin, *Int. J. of Mod. Phys. D* **8**, 291 (1999)
11. D. Novikov, J. Schmalzing, V.F. Mukhanov, *A&A* **364**, 17 (2000)
12. J. Schmalzing and K.M. Górski, *MNRAS* **297**, 355 (1998)
13. S.F. Shandarin, *Soviet Astron. Lett.* **9**, 104 (1983)
14. S.F. Shandarin, *MNRAS* **331**, 865 (2002)
15. S.F. Shandarin and Ya.B. Zel'dovich, *Comments Astrophys.* **10**, 33 (1983)
16. S.F. Shandarin and Ya.B. Zel'dovich, *Phys. Rev. Lett.* **52**, 1488 (1984)
17. S.F. Shandarin, H. Feldman, Y. Xu, M. Tegmark, *ApJS* **141**, 000 (2002) (*astro-ph/0107136*, 2001)
18. M. Tegmark, *Phys. Rev. D* **55**, 5895 (1997)
19. L. Verde, L. Wang, A.F. Heavens, M. Kamionkowski, *MNRAS* **313**, 141 (200)
20. S. Winitzki and A. Kosowsky, *New Astronomy* **3**, 75 (1997)
21. J-H.P. Wu, et al., *Phys. Rev. Lett.* **87**, 251303 (2001)
22. Y. Xu, et al., *Phys. Rev. D* **63**, 103002 (2001)
23. Y. Xu, M. Tegmark, M. and A. de Oliveira-Costa, *Phys. Rev. D* **65**, 083002 (2002)
24. C. Yess and S.F. Shandarin, S.F., *ApJ* **465**, 2 (1996)